Published in final edited form as:
FEBS J. 2008 May ; 275(9): 2305–2314. doi:10.1111/j.1742-4658.2008.06385.x.

Spectroscopic characterization of the oxyferrous complex of prostacyclin synthase in solution and in trapped sol–gel matrix

Hui-Chun Yeh, **Pei-Yung Hsu**, **Ah-Lim Tsai**, and **Lee-Ho Wang**
Division of Hematology, Department of Internal Medicine, University of Texas Health Science Center, Houston, TX, USA

Abstract

Prostacyclin synthase (PGIS) is a member of the cytochrome P450 family in which the oxyferrous complexes are generally labile in the absence of substrate. At 4 °C, the on-rate constants and off-rate constants of oxygen binding to PGIS in solution are 5.9×10^5 $_M^{-1}$ ·s^{-1} and 29 s^{-1}, respectively. The oxyferrous complex decays to a ferric form at a rate of 12 s^{-1}. We report, for the first time, a stable oxyferrous complex of PGIS in a transparent sol–gel monolith. The encapsulated ferric PGIS retained the same spectroscopic features as in solution. The binding capabilities of the encapsulated PGIS were demonstrated by spectral changes upon the addition of O-based, N-based and C-based ligands. The peroxidase activity of PGIS in sol–gel was three orders of magnitude slower than that in solution owing to the restricted diffusion of the substrate in sol–gel. The oxyferrous complex in sol–gel was observable for 24 h at room temperature and displayed a much red-shifted Soret peak. Stabilization of the ferrous–carbon monoxide complex in sol–gel was observed as an enrichment of the 450-nm species over the 420-nm species. This result suggests that the sol–gel method may be applied to other P450s to generate a stable intermediate in the di-oxygen activation.

Keywords

cytochrome P450; eicosanoid; encapsulation; intermediate trapping

Cytochrome P450 (P450) contains a thiolate-ligated heme and catalyzes the hydroxylation, epoxidation, dealkylation, C–C bond scission, dehalogenation and isomerization of a plethora of organic compounds. Typical P450 catalysis involves an oxyferrous intermediate [$Fe(II)O_2$ or $Fe(III)O_2^-\bullet$] that is derived from the di-oxygen binding to the reduced heme iron to initiate the catalytic cycle. The resultant oxyferrous complex is very labile, accepting an electron to elicit the di-oxygen bond scission and producing the iron-oxo species for ensuing reactions, or auto-oxidizing to form the ferric hemoprotein and superoxide anion radical [1]. A method for capturing the intermediate oxyferrous complex is needed to understand P450 di-oxygen activiation in greater detail. Researchers have sought to characterize the thermodynamic and kinetic aspects of this intermediate [2], with the subzero temperature technique being the most widely used approach [3–6]. This procedure slows reaction rates to trap the intermediate within the multiple-step reaction system. For example, Eisenstein *et al.* stabilized the oxyferrous complex of P450cam below −30 °C using a mixed organic solvent system [4]. In the presence and absence of the substrate, the half-life of the oxyferrous complex was 48 and 2.5 h, respectively. Buffer system selection is crucial for this method. Bec *et al.* obtained the oxyferrous complex of P450BM3 under an argon atmosphere at −25 °C in the

Correspondence, L.-H. Wang, Division of Hematology, Department of Internal Medicine, 6431, Fannin, Houston, TX 77030, USA, Fax: +1 713 500 6810, Tel: +1 713 500 6794, lee-ho.wang@uth.tmc.edu.

presence of 50% glycerol [7]. Perera *et al.* also reported the oxyferrous complex of P450BM3 at −55 °C using a glycerol/buffer (70 : 30, v/v) cryosolvent [8]. This low-temperature method can also be used to study subsequent reactions by slowly increasing the temperature [9]. Although the formation of stable oxyferrous complexes can be accomplished by cryotechnique, it is uncertain whether the enzyme behaves in the same manner in the cryosolvent as in an aqueous environment. Additionally, cryotechnique is difficult and sometimes cumbersome.

Proteins encapsulated in transparent sol–gel-derived silica glasses have been shown to retain their spectroscopic properties and to undergo characteristic reactions, making them suitable for optical spectroscopic studies [10]. The sol–gel technique has been applied to many hemoproteins, such as myoglobin [11–14], hemoglobin [11,15–18], cytochrome *c* [11,19,20] and horseradish peroxidase [21,22]. These entrapped proteins were remarkably stable at room temperature and maintained their protein structures, functional activities and spectroscopic properties. The reaction chemistry of the encapsulated enzymes was analogous to that in solution except that the observed rate constant was markedly impeded as a result of diffusional limitation of the reactant. Some transient conformers of the encapsulated hemoglobin and myoglobin were trapped [12,16,23,24]. The reaction intermediates of the encapsulated horseradish peroxidase were characterized at ambient temperature [21]. Although the diffusional limitation inside the porous network (in the case of monoliths) remains an intrinsic obstacle to studying enzymatic intermediates, future developments, such as sol–gel-derived thin films, may allow the use of this technique for broader applications [25]. To date, however, the sol–gel technique has been rarely applied to the study of P450.

Prostacyclin synthase (also known as prostaglandin I_2 synthase; PGIS; EC 5.3.99.4) is located in the membrane of the endoplasmic reticulum and is a downstream enzyme in the prostaglandin synthesis pathway. Unlike other microsomal P450s, PGIS needs neither an oxygen molecule nor an external electron donor for catalysis. In contrast, it catalyzes an isomerization reaction that converts prostaglandin H_2 to prostacyclin, a potent regulator of antiplatelet aggregation and vasodilation. Although PGIS is an atypical P450 with respect to the catalytic reaction, it retains the P450 characteristics of electronic absorption, EPR and magnetic CD spectra [26]. The resting enzyme has a typical low-spin heme with a hydrophobic active site and uses peroxides to bypass the di-oxygen requirement in the ‘peroxide shunt’ reaction [27]. Its crystal structure closely resembles those of other P450s, exhibiting the typical triangular prism-shaped tertiary architecture [28]. Unlike most microsomal P450s, which bind various sizes and shapes of ligands, PGIS has only a few known heme ligands [29]. We have previously developed a heterologous expression system for human PGIS [26]. The availability of a large quantity of homogeneous recombinant PGIS makes it a suitable tool for using to study general P450 features. We chose PGIS for developing the sol–gel method to study P450 enzymes, not only because it has many soluble P450 features but also because it is a membrane-bound P450 and thus may represent microsomal P450s, which are involved in the clearance of most drugs and toxins in humans [30]. In this study, we applied a sol–gel method and demonstrated that entrapped PGIS maintained its spectral features, ligand-binding capabilities and functionality. We also showed that the oxyferrous complex of PGIS in a wet transparent porous silica glass was greatly stabilized in comparison with that in solution, thus establishing the potential of this technique for stabilizing otherwise transient intermediates in the P450 reaction.

Results and Discussion

Formation and decay of oxyferrous PGIS complex in solution

Upon reduction of the ferric PGIS heme by dithionite, the Soret peak was blue-shifted from 418 to 412 nm, accompanied by a decrease in intensity, whereas the Q band (a collective term for the α and β bands), with an α-band peak at 570 nm and a β-band peak at 537 nm, was

replaced with a broad peak at around 550 nm [26]. When the reduced sample was exposed to oxygen, an absorption spectrum of the re-oxidized sample showed the features of the resting enzyme (i.e. a Soret peak at 418 nm and discrete α bands and β bands at 570 and 537 nm, respectively (data not shown), whereas loss of < 5% of the original heme was observed. However, the reduction/oxidation cycle caused no significant loss of enzymatic activity, indicating that the reduction/oxidation cycle of PGIS is a reversible process. This finding is commonly observed in P450s, in which the oxyferrous complex is transient. To examine whether the oxyferrous complex of PGIS is also transient, rapid-scan stopped-flow spectroscopy was performed by mixing ferrous PGIS with air-saturated buffer at 23 °C. The first spectrum recorded after mixing (~ 2.5 ms) had the Soret peak at 420 nm and the Q band exhibiting the maximum at 556 nm and the shoulder at 530 nm (data not shown), similar to most oxyferrous complexes of P450s (Table 1). The 420-nm species then transformed to a species similar to the resting enzyme with the Soret peak at 418 nm and the Q band absorption maxima at 570 and 537 nm. These data also indicated that oxygen binding to ferrous PGIS is a rapid step and is completed within the dead time of the stopped-flow apparatus (i.e. 1.5 ms). In the absence of substrate, the oxyferrous complex of P450 is labile and undergoes auto-oxidation to release superoxide radical and re-establish the resting enzyme [1]. This is probably the case for PGIS. The increase in the absorbance (*A*) at 420 nm, an indication of auto-oxidation, was fit to a single exponential function and a rate constant of $24.8 \pm 0.5\ s^{-1}$ was calculated.

Owing to the difficulty of observing the transition of the ferrous PGIS to oxyferrous PGIS at 23 °C, we performed rapid-scan stopped-flow experiments at 4 °C by reacting 5 μM ferrous PGIS with a fourfold dilution of air-saturated buffer (containing a concentration of ~ 100 μM dissolved oxygen; Fig. 1A). Use of singular value decomposition and global analysis for the model $A \leftrightarrow B \rightarrow C$, with k_1 (forward rate constant of $A \rightarrow B$) equal to $70 \pm 9\ s^{-1}$, k_2 (backward rate constant of $A \leftarrow B$) equal to $30 \pm 6\ s^{-1}$, and k_3 (forward rate constant of $B \rightarrow C$) equal to $20 \pm 2\ s^{-1}$, yielded the spectra of individual intermediates shown in Fig. 1B. The conversion of species A to species B resulted in a slight increase of the Soret peak that was accompanied by a peak shift from 416 to 422 nm. Moreover, in species B the intensity of the α band (556 nm) was greater than that of the β band (530 nm). This spectral feature is similar to that of oxyferrous complexes of P450s, particularly at the Q band region in which the α band has a slightly higher intensity than the β band. Species C is the re-oxidized ferric PGIS. To characterize kinetically the binding step, a series of stopped-flow experiments was carried out at 4 °C in which the ferrous PGIS was mixed with varying ratios of air-saturated and nitrogen-saturated buffer. The oxygen-binding and subsequent decay steps were monitored at 430 nm and 420 nm, respectively. The slope of the observed pseudo-first-order rate constants versus the oxygen concentration gives a second-order rate constant of $5.9 \pm 0.2 \times 10^5\ M^{-1} \cdot s^{-1}$ (Fig. 1C). A dissociation rate constant of $29 \pm 3\ s^{-1}$ was obtained from the ordinate intercept. The oxyferrous PGIS, however, was unstable and readily oxidized to the resting PGIS at a decay rate of $12 \pm 2\ s^{-1}$ ($t_{1/2}$ ~ 0.06 s) at 4 °C in an oxygen concentration-independent manner. The concentration-independent slow phase was consistent with the auto-oxidation step that leads to the production of the superoxide radical and resting enzyme. It should be noted that our knowledge about the oxyferrous intermediate in microsomal P450 catalysis is generally hampered by heterogeneous kinetic properties, partly as a result of the presence of heterogeneous populations of aggregated P450 forms. Using the monomeric and monodispersive PGIS [28], we provided clear information for the oxyferrous intermediate of a microsomal P450 enzyme. All our data fit well to the simple scheme of $Fe^{2+} + O_2 \leftrightarrow [\text{oxyferrous}] \rightarrow Fe^{3+} + O_2^- \bullet$. Taken together, the binding of oxygen to ferrous PGIS is similar to that of other P450s with respect to the transient formation of the oxyferrous form, followed by restoration of the resting enzyme and superoxide radical anion formation.

Table 2 shows the second-order rate constants of oxygen binding to the ferrous P450s as well as the dissociation constants and auto-oxidation rates of their oxyferrous complexes. The

oxyferrous complex was much less stable and readily auto-oxidized in the absence of substrate. In P450 hydroxylation, binding of the substrate generally induces a five-coordinate/high-spin heme. Lacking the knowledge of such a substrate for PGIS, we only examined the complex in the substrate-free form. The second-order rate constant of oxygen binding to PGIS at 4 °C was $5.9 \times 10^5\ _M{}^{-1}{\cdot}s^{-1}$ and the auto-oxidation rate constant was 12 s^{-1}. These values are comparable to those obtained from the microsomal CYP3A4 assembled in a lipid bilayer of 10-nm diameter (Nanodiscs) as a soluble and monomeric entity [31]. CYP3A4 in Nanodiscs is monodisperse and kinetically homogeneous. Upon oxygen binding, ferrous CYP3A4 in the substrate-free form showed a red-shift of the Soret peak to 418 nm with a fused Q band peak near 552 nm, whereas in the presence of testosterone the Soret peak was further red-shifted to around ~ 424 nm. In the presence of substrate, the second-order rate constant of oxygen binding at 6 °C was $5 \times 10^5\ _M{}^{-1}{\cdot}s^{-1}$, and the auto-oxidation rate of the oxyferrous complex was 0.37 s^{-1}. In the absence of substrate, the auto-oxidation rate was 20 s^{-1} at 5 °C. Compared with bacterial P450s, such as P450cam and P450BM3, the auto-oxidation of PGIS and CYP3A4 occurred approximately three to four orders of magnitude faster. This may explain why bacterial P450s generally use their redox equivalents more efficiently than do microsomal P450s, which exhibit a higher degree of uncoupling and a greater production of superoxide radical anion or hydrogen peroxide. Although PGIS does not need an oxygen molecule for catalysis, it may serve as a model for studying oxyferrous intermediates of microsomal P450s.

UV/VIS spectra of ligand binding of PGIS in solution and in sol–gel monolith

In an attempt to stabilize the oxyferrous complex of PGIS for further studies, we adopted a method that immobilized the protein in sol–gel-derived silica glasses. The encapsulated PGIS has a Soret peak at 418 nm and α and β bands at 571 and 537 nm, respectively, which are similar to PGIS in solution (Fig. 3A, solid line). Spectral perturbation was then used to examine whether the encapsulated PGIS interacted with the heme ligands. We chose U46619 (an O-based ligand; a substrate analog whose oxygen atom at the C9 position is replaced with a carbon atom), NaCN (a C-based ligand) and clotrimazole (an N-based ligand) as the probes because they induced distinct patterns of spectral changes [26]. Figure 2A shows the difference spectra of U46619 binding to PGIS in solution and in sol–gel. In solution, U46619 binding caused a blue shift of the Soret peak (upper left panel). The difference spectrum shows the peak at 410 nm and the trough at 428 nm (bottom left panel). Similarly, binding of U46619 to the encapsulated PGIS caused a blue shift of the Soret band, although to a lesser extent (upper right panel), and generated a difference spectrum with the peak at 406 nm and the trough at 426 nm (lower right panel). Results of the binding of NaCN and clotrimazole to PGIS in solution and in sol–gel are shown in Figs 2B,C. NaCN induced a red shift of the Soret peak in both aqueous and encapsulated PGIS (Fig. 2B, upper panels). Spectral perturbation by NaCN in solution produced a peak at 443 nm and a trough at 416 nm, and in sol–gel, a peak at 444 nm and a trough at 416 nm (Fig. 2B, bottom panels). Binding of clotrimazole to aqueous PGIS produced spectral changes identical to those of encapsulated PGIS, with a peak at 433 nm and a trough at 414 nm (Fig. 2C). These results indicate that the substrate access channel, active site and heme structure of PGIS in solution are preserved in the sol–gel matrix.

Peroxidase reactivity of PGIS in solution and sol–gel

Similarly to other P450s, PGIS possesses peroxidase activity that uses peroxides as the substrate [26]. Because prostaglandin H_2 is unstable in aqueous solution, we tested the enzymatic activity of encapsulated PGIS using peracetic acid as the substrate and guaiacol as the cosubstrate. Enzymatic activity was followed by absorbance changes at 470 nm that monitored the oxidation of guaiacol. Upon the addition of peracetic acid to encapsulated PGIS, the orange product first appeared at the outer face of the monolith and gradually disappeared, accompanied by the formation of fresh orange product in the inner layer during the 30-min incubation. This result indicates not only that encapsulated PGIS was active but also that

activity was limited by diffusion of the substrate. We also estimated the enzyme activities of aqueous PGIS and encapsulated PGIS using the same concentration of guaiacol and peracetic acid. The initial rates of the aqueous and encapsulated PGIS were 59.4 and 0.06 mole product/mole PGIS/min, respectively, indicating a difference of three orders of magnitude in the catalytic activity of the two forms of PGIS. It should be noted that because only a small fraction of encapsulated PGIS is involved in the catalysis, the catalytic rate determined is substantially decreased.

Binding of O_2 to PGIS in the sol–gel monolith

We further studied O_2 binding to encapsulated PGIS. After adding dithionite to buffer containing encapsulated PGIS, we anticipated fully reduced PGIS with the Soret peak at 412 nm, as in solution [26]. However, in contrast, the Soret peak gradually shifted over a 4-h incubation time from 418 to 425 nm with the formation of well-defined α bands and β bands at 558 and 530 nm, respectively (Fig. 3A). This spectral feature is somewhat similar to the oxyferrous complex resolved by stopped-flow spectroscopy (Fig. 1B, dotted line), except that the Soret peak is further red-shifted. We speculated that the oxyferrous complex was formed upon the reduction of PGIS because certain amounts of oxygen were cotrapped with PGIS in sol–gel. To test this, we first bubbled N_2 gas into the gel-containing solution for 2 h to remove trapped oxygen prior to the addition of dithionite. The spectrum of reduced PGIS in sol–gel with the Soret peak at 413 nm and the fused Q band (Fig. 3B, right panel, dashed line) is very similar to that of reduced PGIS in solution (Fig. 3B, left panel, dotted line). Reduced PGIS in sol–gel was then soaked in an air-saturated buffer overnight. Consequently, the encapsulated PGIS displayed a Soret peak at 417 nm with separated α bands and β bands (Fig. 3B, right panel, dash-dotted line), indicating that PGIS was re-oxidized to the ferric form. Notably, the re-oxidized PGIS lost approximately 10% of the intensity of the Soret peak, suggesting that the redox process may cause bleaching of the enzyme. We then added a small amount of dithionite to the solution containing re-oxidized PGIS and sealed the cuvette with parafilm. Again, the Soret peak was gradually red-shifted and after 4 h of incubation it reached 422 nm, whereas the α bands and β bands were 557 and 528 nm, respectively (Fig. 3B, right panel, thick solid line). This spectral feature is similar to the oxyferrous PGIS in sol–gel shown in Fig. 3A, suggesting that oxygen trapped in the sol–gel is capable of forming the oxyferrous PGIS complex. Incomplete red-shift of the Soret peak may be caused by the presence of a ferric form that was not reduced as a result of the smaller amount of trapped oxygen. This result also suggests that the redox process in the encapsulated PGIS is reversible. The oxyferrous complex was stable for more than 24 h at room temperature, indicating that the rate of auto-oxidation in sol–gel is about six orders of magnitude slower than that observed in solution.

The Soret peak of the oxyferrous PGIS determined in this study varied from 420 nm at 23 °C to 422 nm at 4 °C in solution and to 425 nm in sol–gel at 23 °C. However, all values fell within the range of Soret peaks reported for the other oxyferrous P450s (i.e. 417–428 nm; Table 1). The transient nature of the complex may make it difficult to obtain the spectrum of the pure oxyferrous form [32]. As a result, the resolved oxyferrous spectrum obtained by global analysis contains a mixture of the ferrous, oxyferrous and ferric forms. Interestingly, a more long-lived oxyferrous complex, such as that in the presence of the substrate or at lower temperature, tends to have a more red-shifted Soret peak (Table 1). This trend suggests that the Soret peak of the oxyferrous complex is probably at a higher wavelength, as the peaks for the ferric and ferrous heme are located at shorter wavelengths. Our results also support this idea and thus demonstrate that the oxyferrous complex of PGIS is more stable in sol–gel than in solution. Although the association rate of oxygen and ferrous PGIS was decreased in sol–gel, the two processes that dissipate the oxyferrous intermediate (i.e. back dissociation to ferrous heme and chemical decay to ferric heme) must be slowed considerably in the sol–gel environment to allow more accumulation of the oxyferrous intermediate, thus maximizing the red-shift of the Soret peak.

Binding of CO to PGIS in sol–gel monolith

To test whether this technique can be applied to other gaseous ligands, we bubbled carbon monoxide into buffer containing encapsulated PGIS for 1 h and then added dithionite to the solution. The spectrum showed Soret peaks at 422 and 450 nm (Fig. 4), similar to those observed in solution [26]. Our previous study has shown that while the formation rate of the ferrous–CO complex of PGIS (5.6×10^5 $_M^{-1} \cdot s^{-1}$) falls within the ranges of most P450s, the complex is surprisingly unstable, converting to a 422-nm species at a rate of 0.7 s^{-1}. In sol–gel, we observed a slower formation of the complex, requiring 20 min to reach λ_{450} maximum. Furthermore, the complex was stable in sol–gel for at least 2.5 h, indicating that the ferrous–CO complex is greatly stabilized in sol–gel, a trend similar to that observed for the ferrous–O_2 complex.

In conclusion, transient intermediates that are difficult to achieve in aqueous solution were produced and stabilized using this technique. PGIS was encapsulated in a silica matrix with minimal changes to its spectroscopic properties, allowing us to study trapped intermediates. The spectral data obtained in this study demonstrated, for the first time, the existence of the oxyferrous PGIS complex and evidence for its similarity to other P450s. This method can be applied to other spectroscopy, such as resonance Raman and magnetic CD, for characterization of the oxyferrous and reduced–CO complexes and, potentially, for other intermediates in the P450 reaction cycle.

Experimental procedures

Materials

Purified recombinant PGIS, modified to be soluble by deletion of the amino-terminal membrane-binding domain, was prepared as previously described [28]. Tetramethyl orthosilicate (TMOS), sodium cyanide, clotrimazole and sodium dithionite were purchased from Sigma-Aldrich (St Louis, MO, USA) and used without further purification. UV-grade polymethyl methacrylate disposable cuvettes (10 mm × 4 mm × 45 mm; 1.5 mL; 280–800 nm) were purchased from VWR (West Chest, PA, USA). U46619 (15-hydroxy-9,11-[methanoepoxy] prosta-5,13-dienoic acid) was obtained from Cayman (Ann Arbor, MI, USA).

Preparation of sol–gel-encapsulated PGIS

TMOS sol was prepared by the sonication of 1.5 mL of TMOS, 0.35 mL of water and 0.01 mL of 0.1 M HCl for 30 min [10]. TMOS-derived monoliths were prepared as described previously, with slight modifications [21]. Briefly, 0.24 mL of TMOS sol was mixed with 0.39 mL of buffer (20 mm Na/P_i, pH 7.5, and 10% glycerol) containing approximately 20 μM PGIS. The mixture was placed in a polymethyl methacrylate cuvette, and the monoliths formed within 60 min. For 2 weeks following gelation, TMOS-derived monoliths (2 mm × 7 mm × 14 mm) were rinsed three times daily with 1 mL of buffer to remove methanol produced during gelation and were stored in buffer at 4 °C. The lifetime of encapsulated PGIS was more than 6 months.

Ligand binding

U46619, NaCN and clotrimazole were prepared as stock solutions in 20 mM Na/P_i (pH 7.5) and 10% glycerol. Aliquots of the ligand stock were added in 1 mL of buffer containing either aqueous PGIS or encapsulated PGIS. Spectra were taken before and after ligand addition. Because of the slow diffusion rate, a 20 min incubation of the PGIS monolith was required. Spectra were recorded using a Shimadzu UV-2501PC spectrophotometer (Kyoto, Japan). Difference spectra were generated by subtraction of the spectrum of PGIS from each ligand-bound spectrum.

Stopped-flow kinetic measurements

PGIS (10 μm) in 20 m_M Na/P_i (pH 7.4) and 10% glycerol was introduced in a tonometer. The tonometer was processed by five cycles of alternating vacuum (30 s) and argon replacement (5 min) through a glass valve connected to an anaerobic train. PGIS was then reduced with the stepwise addition of dithionite through a gas-tight Hamilton syringe attached to the tonometer. Absorption spectra were recorded after each addition of dithionite to ensure complete conversion from the ferric form to the ferrous form. O_2-saturated solution (400 μ_M at 4 °C) was prepared by continuous bubbling with O_2 for more than 20 min and bubbling between each measurement. The O_2 solutions were prepared by diluting O_2-saturated buffer into nitrogen-saturated buffer with a gas-tight syringe through a rubber septum. The PGIS-containing tonometer and O_2 solution syringe were loaded on a Bio-Sequential DX-18MV stopped-flow apparatus (Applied Photophysics, Leather-head, UK) equipped with a temperature-controlled circulator. Heme spectral changes upon O_2 binding were monitored at 4 °C with either photodiode array detection or single wavelength measurement. For single wavelength kinetic data, the built-in software was used for rate analysis. The rapid-scan data were analyzed using the PRO-K software package (Applied Photophysics).

Preparation of O_2-bound ferrous PGIS monoliths

TMOS-derived PGIS monoliths were placed in a quartz cuvette containing 1 mL of buffer. The cuvette was sealed with parafilm after adding 10 μL of 0.1 $mg \cdot mL^{-1}$ sodium dithionite stock solution. Spectra were taken before and after the addition of sodium dithionite.

Peroxidase activity

The peroxidase reaction was initiated by adding peracetic acid (100 μ_M) into the guaiacol solution (1.78 m in 20 m_M Na/P_i, pH 7.5, with 10% glycerol) containing either aqueous PGIS (0.5 μm) or encapsulated PGIS. To reach equilibrium, guaiacol and PGIS monoliths were incubated for 30 min before adding peracetic acid. Guaiacol oxidation was monitored by measuring the change in absorbance at 470 nm at a temperature of 23 °C ($\varepsilon = 26.6$ $m_M^{-1} \cdot cm^{-1}$) [33]. Control experiments without PGIS were used to correct for noncatalytic background oxidation.

Abbreviations

P450	cytochrome P450
PGIS	prostaglandin I_2 synthase or prostacyclin synthase
TMOS	tetramethyl orthosilicate

Acknowledgments

This work was supported by Grants HL60625 (to L.-H. W.) and GM44911 (to A.-L. T.) from the National Institutes of Health. We thank Dr Wann-Yin Lin at the National Taiwan University for encouragement and helpful discussion in sol–gel preparation and Dr Jinn-Shyan Wang of the Fu Jen Catholic University for assistance in the stopped-flow experiments during his sabbatical leave.

References

1. Sligar SG, Lipscomb JD, Debrunner PG, Gunsalus IC. Superoxide anion production by the autoxidation of cytochrome P450cam. Biochem Biophys Res Commun 1974;61:290–296. [PubMed: 4441397]
2. Guengerich FP, Ballou DP, Coon MJ. Spectral intermediates in the reaction of oxygen with purified liver microsomal cytochrome P-450. Biochem Biophys Res Commun 1976;70:951–956. [PubMed: 938535]

3. Begard E, Debey P, Douzou P. Sub-zero temperature studies of microsomal cytochrome P-450: interaction of Fe2+ with oxygen. FEBS Lett 1977;75:52–54. [PubMed: 852592]
4. Eisenstein L, Debey P, Douzou P. P450cam: oxygenated complexes stabilized at low temperature. Biochem Biophys Res Commun 1977;77:1377–1383. [PubMed: 901539]
5. Bonfils C, Debey P, Maurel P. Highly purified microsomal P-450: the oxyferro intermediate stabilized at low temperature. Biochem Biophys Res Commun 1979;88:1301–1307. [PubMed: 38784]
6. Larroque C, Van Lier JE. The subzero temperature stabilized oxyferro complex of purified cytochrome P450scc. FEBS Lett 1980;115:175–177. [PubMed: 7398873]
7. Bec N, Anzenbacher P, Anzenbacherova E, Gorren AC, Munro AW, Lange R. Spectral properties of the oxyferrous complex of the heme domain of cytochrome P450 BM-3 (CYP102). Biochem Biophys Res Commun 1999;266:187–189. [PubMed: 10581187]
8. Perera R, Sono M, Raner GM, Dawson JH. Subzero-temperature stabilization and spectroscopic characterization of homogeneous oxyferrous complexes of the cytochrome P450 BM3 (CYP102) oxygenase domain and holoenzyme. Biochem Biophys Res Commun 2005;338:365–371. [PubMed: 16197919]
9. Davydov R, Makris TM, Kofman V, Werst DE, Sligar SG, Hoffman BM. Hydroxylation of camphor by reduced oxy-cytochrome P450cam: mechanistic implications of EPR and ENDOR studies of catalytic intermediates in native and mutant enzymes. J Am Chem Soc 2001;123:1403–1415. [PubMed: 11456714]
10. Ellerby LM, Nishida CR, Nishida F, Yamanaka SA, Dunn B, Valentine JS, Zink JI. Encapsulation of proteins in transparent porous silicate glasses prepared by the sol-gel method. Science 1992;255:1113–1115. [PubMed: 1312257]
11. Wu S, Lin J, Chan SI. Oxidation of dibenzothiophene catalyzed by heme-containing enzymes encapsulated in sol-gel glass. A new form of biocatalysts. Appl Biochem Biotechnol 1994;47:11–20. [PubMed: 8203869]
12. Shibayama N, Saigo S. Oxygen equilibrium properties of myoglobin locked in the liganded and unliganded conformations. J Am Chem Soc 2003;125:3780–3783. [PubMed: 12656610]
13. Ray A, Feng M, Tachikawa H. Direct electrochemistry and Raman spectroscopy of sol-gel-encapsulated myoglobin. Langmuir 2005;21:7456–7460. [PubMed: 16042479]
14. Dantsker D, Samuni U, Friedman JM, Agmon N. A hierarchy of functionally important relaxations within myoglobin based on solvent effects, mutations and kinetic model. Biochim Biophys Acta 2005;1749:234–251. [PubMed: 15914102]
15. Juszczak LJ, Friedman JM. UV resonance Raman spectra of ligand binding intermediates of sol-gel encapsulated hemoglobin. J Biol Chem 1999;274:30357–30360. [PubMed: 10521410]
16. Samuni U, Dantsker D, Khan I, Friedman AJ, Peterson E, Friedman JM. Spectroscopically and kinetically distinct conformational populations of sol-gel-encapsulated carbonmonoxy myoglobin. A comparison with hemoglobin. J Biol Chem 2002;277:25783–25790. [PubMed: 11976324]
17. Samuni U, Friedman JM. Proteins in motion: resonance Raman spectroscopy as a probe of functional intermediates. Methods Mol Biol 2005;305:287–300. [PubMed: 15940003]
18. Shibayama N, Saigo S. Fixation of the quaternary structures of human adult haemoglobin by encapsulation in transparent porous silica gels. J Mol Biol 1995;251:203–209. [PubMed: 7643396]
19. Fiandaca G, Vitrano E, Cupane A. Ferricytochrome c encapsulated in silica nanoparticles: structural stability and functional properties. Biopolymers 2004;74:55–59. [PubMed: 15137094]
20. Droghetti E, Smulevich G. Effect of sol-gel encapsulation on the unfolding of ferric horse heart cytochrome c. J Biol Inorg Chem 2005;10:696–703. [PubMed: 16184400]
21. Smith K, Silvernail NJ, Rodgers KR, Elgren TE, Castro M, Parker RM. Sol-gel encapsulated horseradish peroxidase: a catalytic material for peroxidation. J Am Chem Soc 2002;124:4247–4252. [PubMed: 11960453]
22. Hungerford G, Rei A, Ferreira MI, Suhling K, Tregidgo C. Diffusion in a sol-gel-derived medium with a view toward biosensor applications. J Phys Chem B 2007;111:3558–3562. [PubMed: 17388494]
23. Shibayama N. Functional analysis of hemoglobin molecules locked in doubly liganded conformations. J Mol Biol 1999;285:1383–1388. [PubMed: 9917383]

24. Shibayama N, Saigo S. Direct observation of two distinct affinity conformations in the T state human deoxyhemoglobin. FEBS Lett 2001;492:50–53. [PubMed: 11248235]
25. Gupta R, Chaudhury NK. Entrapment of biomolecules in sol-gel matrix for applications in biosensors: problems and future prospects. Biosens Bioelectron 2007;22:2387–2399. [PubMed: 17291744]
26. Yeh HC, Hsu PY, Wang JS, Tsai AL, Wang LH. Characterization of heme environment and mechanism of peroxide bond cleavage in human prostacyclin synthase. Biochim Biophys Acta 2005;1738:121–132. [PubMed: 16406803]
27. Yeh H-C, Tsai A-L, Wang L-H. Reaction mechanisms of 15-hydroperoxyeicosatetraenoic acid catalyzed by human prostacyclin and thromboxane synthases. Arch Biochem Biophys 2007;461:159–168. [PubMed: 17459323]
28. Chiang CW, Yeh HC, Wang LH, Chan NL. Crystal structure of the human prostacyclin synthase. J Mol Biol 2006;364:266–274. [PubMed: 17020766]
29. Ullrich V, Brugger R. Prostacyclin and thromboxane synthase: new aspects of hemethiolate catalysis. Angew Chem Int Ed Engl 1994;33:1911–1919.
30. Johnson EF. The 2002 Bernard B. Brodie Award lecture: deciphering substrate recognition by drug-metabolizing cytochromes P450. Drug Metab Dispos 2003;31:1532–1540. [PubMed: 14625350]
31. Denisov IG, Grinkova YV, Baas BJ, Sligar SG. The ferrous-dioxygen intermediate in human cytochrome P450 3A4. Substrate dependence of formation and decay kinetics. J Biol Chem 2006;281:23313–23318. [PubMed: 16762915]
32. Berka V, Yeh HC, Gao D, Kiran F, Tsai AL. Redox function of tetrahydrobiopterin and effect of L-arginine on oxygen binding in endothelial nitric oxide synthase. Biochemistry 2004;43:13137–13148. [PubMed: 15476407]
33. Baldwin DA, Marques HM, Pratt JM. Hemes and hemoproteins. 5: Kinetics of the peroxidatic activity of microperoxidase-8: model for the peroxidase enzymes. J Inorg Biochem 1987;30:203–217. [PubMed: 2821191]
34. Peterson JA, Ishimura Y, Griffin BW. *Pseudomonas putida* cytochrome P-450: characterization of an oxygenated form of the hemoprotein. Arch Biochem Biophys 1972;149:197–208. [PubMed: 4335959]
35. Sono M, Perera R, Jin S, Makris TM, Sligar SG, Bryson TA, Dawson JH. The influence of substrate on the spectral properties of oxyferrous wild-type and T252A cytochrome P450-CAM. Arch Biochem Biophys 2005;436:40–49. [PubMed: 15752707]
36. Tuckey RC, Kamin H. The oxyferro complex of adrenal cytochrome P-450scc. Effect of cholesterol and intermediates on its stability and optical characteristics. J Biol Chem 1982;257:9309–9314. [PubMed: 7107571]
37. Oprian DD, Gorsky LD, Coon MJ. Properties of the oxygenated form of liver microsomal cytochrome P-450. J Biol Chem 1983;258:8684–8691. [PubMed: 6863307]
38. Lambeir A-M, Appleby CA, Dunford HB. The formation and decay of the oxyferrous forms of the cytochromes P450 isolated from *Rhizobium japonicum*. Rapid spectral scan and stopped-flow studies. Biochem Biophys Acta 1985;828:144–150.
39. Denisov IG, Dawson JH, Hager LP, Sligar SG. The ferric-hydroperoxo complex of chloroperoxidase. Biochem Biophys Res Commun 2007;363:954–958. [PubMed: 17920039]
40. Lambeir AM, Dunford HB. Oxygen binding to dithionite-reduced chloroperoxidase. Eur J Biochem 1985;147:93–96. [PubMed: 3971978]
41. Tuckey RC, Kamin H. Kinetics of O_2 and CO Binding to adrenal cytochrome P-450scc. Effect of cholesterol, intermediates, and phosphatidylcholine vesicles. J Biol Chem 1983;258:4232–4237. [PubMed: 6833254]
42. Kashem MA, Dunford HB. The formation and decay of the oxyferrous complex of beef adrenocortical cytochrome P-450scc. Rapid-scan and stopped-flow studies. Biochem Cell Biol 1987;65:486–492. [PubMed: 3620163]
43. Bonfils C, Balny C, Maurel P. Direct evidence for electron transfer from ferrous cytochrome b5 to the oxyferrous intermediate of liver microsomal cytochrome P-450 LM2. J Biol Chem 1981;256:9457–9465. [PubMed: 7287694]
44. Rosen P, Stier A. Kinetics of CO and O_2 complexes of rabbit liver microsomal cytochrome P 450. Biochem Biophys Res Commun 1973;51:603–611. [PubMed: 4145062]

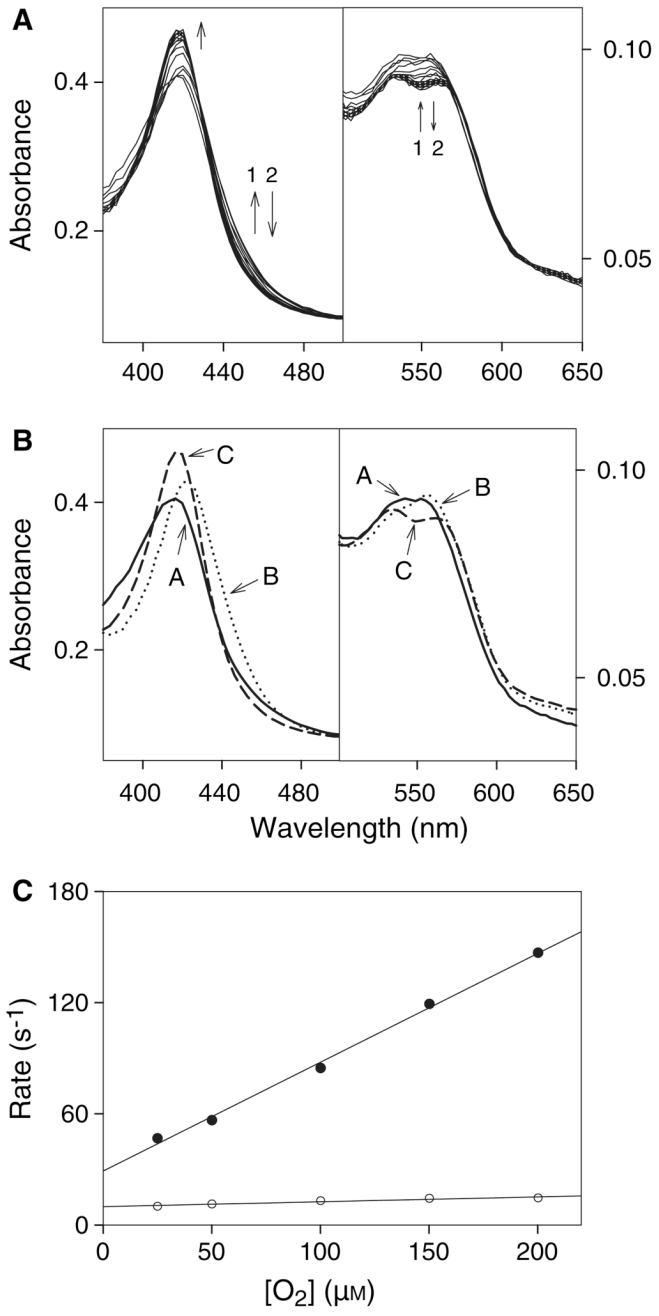

Fig. 1.

Stopped-flow study of ferrous PGIS reaction with oxygen. (A) Rapid scan absorbance spectral changes for the reaction of ferrous PGIS (5 μM) with oxygenated buffer (100 μM) at 4 °C. Spectra were recorded at 0.0013, 0.0064, 0.014 and 0.0127 s, and then at increments of 0.026-s intervals until 1 s of reaction time had been monitored. Arrows show the directions of spectral changes with increasing time, and numbers indicate the orders of the signal change. (B) Spectral intermediates resolved by global analysis using the sequential model of A ↔ B→C (species A, solid line; species B, dotted line; species C, dashed line). (C) Plots of the observed rate constants for the first phase (filled circles) and the second phase (open circles) versus oxygen

concentration. Experiments were carried out by mixing ferrous PGIS (5.0 μM) with various concentrations of oxygenated buffer (25–200 μM).

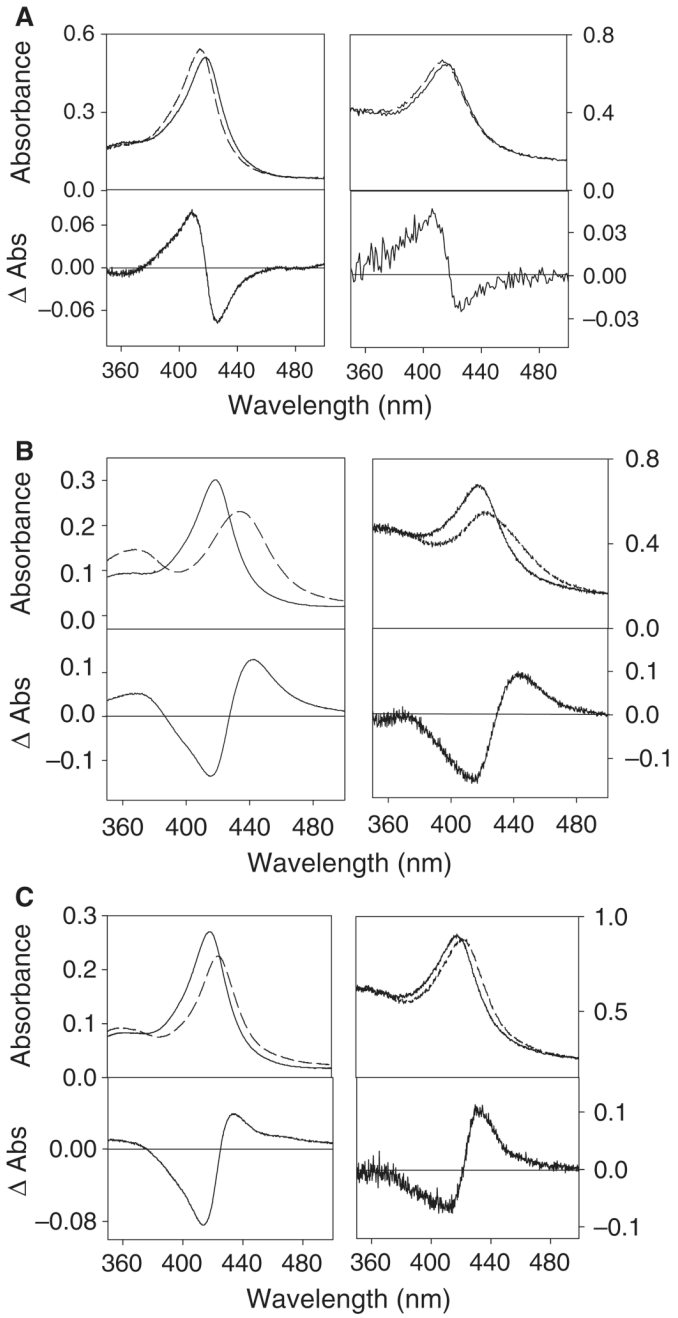

Fig. 2.

Absorption spectra of PGIS and its ligand complexes in solution and in sol–gel. Binding with (A) U46619, (B) NaCN and (C) clotrimazole. Spectra were recorded before (solid lines) and after (dashed lines) addition of the exogeneous ligands into the aqueous PGIS (left panels) and encapsulated PGIS (right panels). For each ligand, the absolute absorption spectrum is shown in the top panel and the difference spectra in the bottom panel.

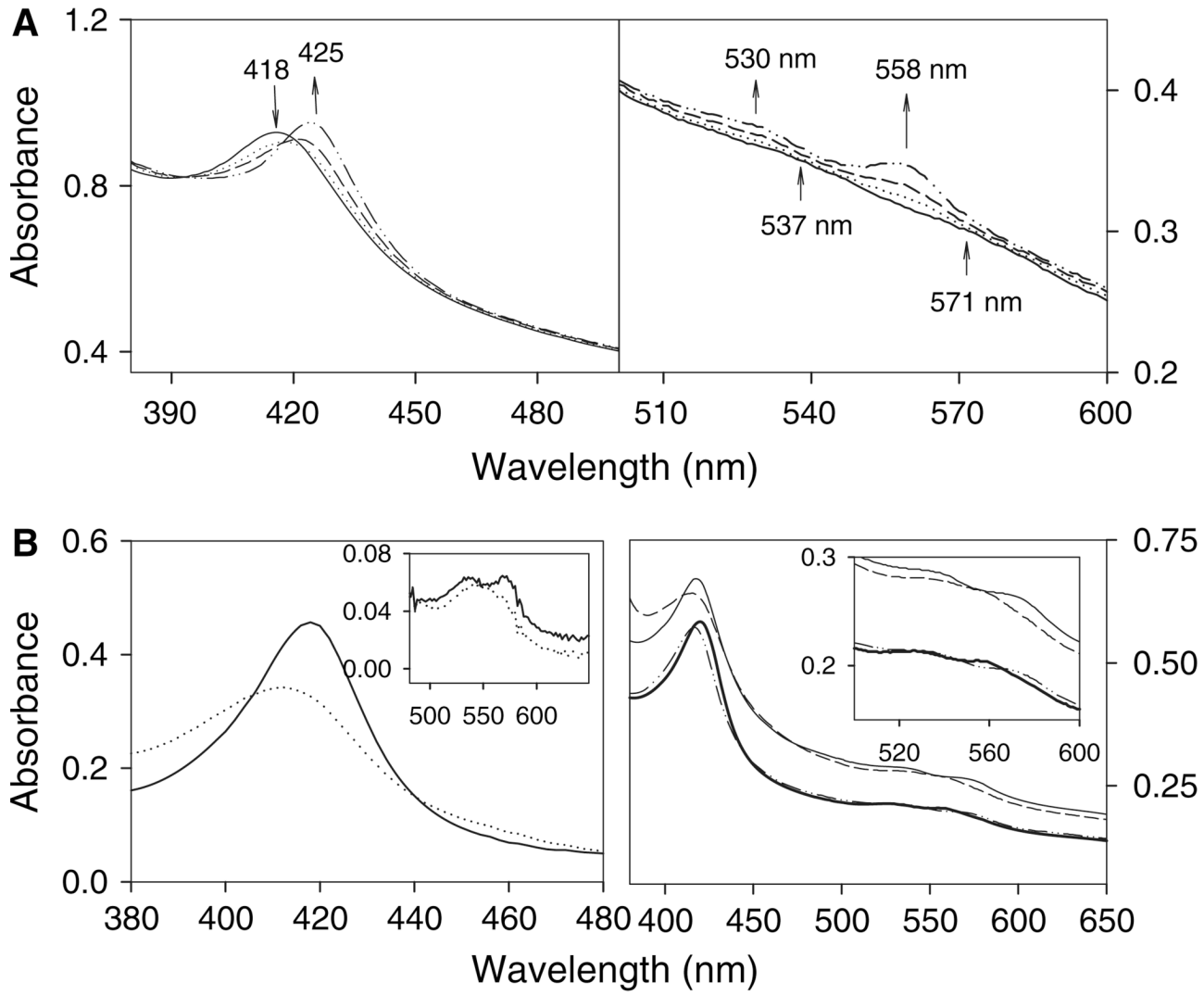

Fig. 3.

Comparison of oxyferrous PGIS complexes in solution and in sol–gel. (A) Absorption spectra of PGIS (solid line) and its oxyferrous complex formed at 1.5 h (dotted line), 2.5 h (dashed line) and 4 h (dot–dot–dash line) in the sol–gel. (B) Left panel, absorption spectra of 4.6 μM ferric PGIS (solid line) and ferrous PGIS (dotted line) in solution. Right panel, ferric PGIS (thin solid line), ferrous PGIS (dashed line), re-oxidized PGIS (dash-dot-dot line) and oxyferrous PGIS (thick solid line) in sol–gel.

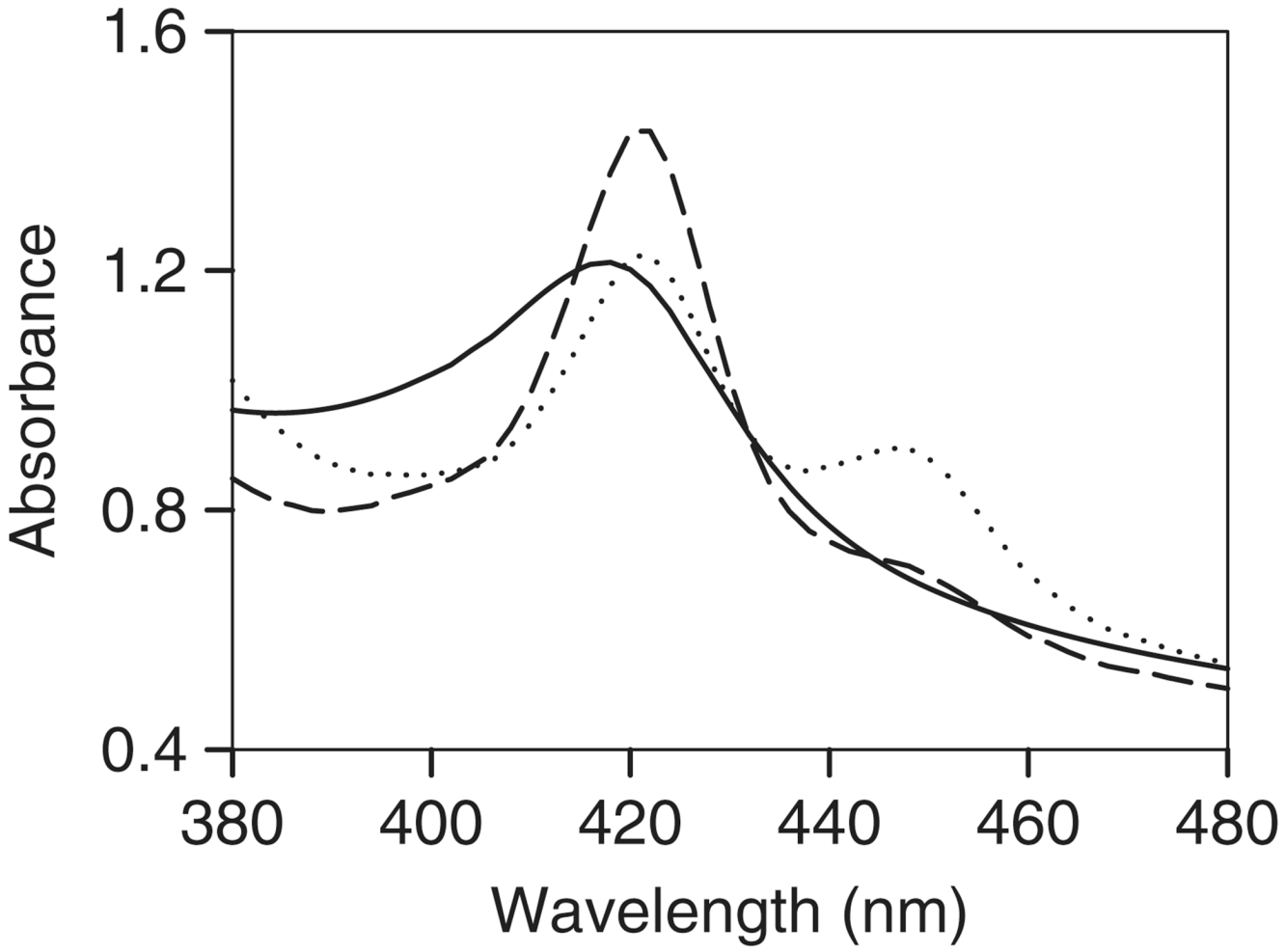

Fig. 4.

Progression of ferrous–CO complex formation in sol–gel. Ferric PGIS (solid line), a ferrous–CO complex of 20 min of incubation (dotted line) and a ferrous–CO complex of 2.5 h of incubation (dashed line) in sol–gel.

Table 1

Spectral properties of the oxyferrous complexes of PGIS in comparison with other P450s. Temp., temperature.

	Soret	β / α band	Temp. (°C)	Reference
PGIS (sol–gel)	425	530 / 558	23	This study
PGIS (solution)	420	530 / 556	23	This study
PGIS (solution)	422	530 / 556	4	This study
P450BM3 + arachidonic acid	423	560	−55	[8]
P450cam				
+ camphor	418	555	4	[34]
+ camphor	418	552	−20	[4]
+ camphor	420	553	−40	[35]
− camphor	418	552	−40	[4]
P4503A4				
− testosterone	418	552	6	[31]
+ testosterone	424		6	[31]
Adrenal cortex mitochondria P450scc				
+ cholesterol	423	553	−17	[36]
+ cholesterol	422	555	−30	[6]
− cholesterol	420	555	−17	[36]
Hepatic microsomes				
$P450_{LM2}$	422	557–558	−30	[5]
$P450_{LM3b}$	418	555	10	[37]
$P450_{LM4}$	418	555	10	[37]
Rhizobium				[38]
P450a	417		4	
P450b	419		4	
P450c	421		4	
Caldariomyces fumago				
Chloroperoxidase	428	553 / 587	< −103	[39]
Chloroperoxidase	428	555 / 588	25	[40]
Nitric oxide synthase				
+ arginine	428	~ 560	4	[32]
− arginine	418	~ 560	4	[32]

Table 2

Kinetic constants of the formation and decay of the oxyferrous complexes for the reaction of oxygen with various ferrous P450s[a]. Temp., temperature.

	k_{on} ($M^{-1}·s^{-1}$)	k_{off} (s^{-1})	K_d (μM)	k_{decay} (s^{-1})	Temp. (°C)
PGIS (this study)	5.9×10^5	29	49	12	4
P4503A4 [31]					
+ testosterone	5.0×10^5			0.37	6
− testosterone				20	5
Rhizobium [38]					
P450a	5×10^5			2.2	4
P450b	7×10^5			1.6	4
P450c	7×10^5			4.8	4
Pseudomonas putida P450cam [4,34]					
+ camphor	7.7×10^5 (4 °C)		1.4	0.55×10^{-3}	2
− camphor	Very fast			1.8×10^{-3}	2
Adrenal cortex mitochondria P450scc [36,41,42]					
+ cholesterol	3.8×10^5	4.7	12	6.3	4
+ cholesterol	1.3×10^6 (8 °C)		23	6.1×10^{-3}	2
− cholesterol	Very fast			4.0×10^{-3}	−17
Hepatic microsomes [37,43,44]					
$P450_{LM2}$	4.4×10^6 (25 °C)			3.7	2
$P450_{LM3}$	~ 10^6 (25 °C)			4.3	10
$P450_{LM4}$	5.0×10^5		0.7	0.9	10
Caldariomyces fumago [40]					
Chloroperoxidase (pH 2.8–6.8)	5.5×10^5	8–32	10–70		25
Nitric oxide synthase [32]					
+ arginine	4×10^5	5.5	13.8	1.4	4
− arginine	1.4×10^5	60	43	5–30	4

[a]Unless otherwise indicated, the experiments were carried out at a pH of 7.1–7.5.